

# Accurate Estimation of Digital Communication System Metrics — SNR, EVM and $\rho$ in a Nonlinear Amplifier Environment

Khaled M. Gharaibeh, Kevin G. Gard and Michael B. Steer

Dept. of Electrical and Computer Engineering, North Carolina State University, Raleigh, NC 27695  
Tel. 919-515-5191, FAX 919-515-2285, e-mail: {kmgharai,kggard,mbs}@ncsu.edu

**Abstract** - A nonlinear spectral analysis technique that enables digital communication system metrics; SNR, EVM and the waveform quality factor ( $\rho$ ) to be related to in-band distortion spectrum is presented. System metrics are estimated from the measured output power and in-band distortion power. The estimated metrics are verified by direct measurements of each metric using a Vector Signal Analyzer (VSA) performed on a forward-link IS-95 signal. Estimated system metrics are in excellent agreement with measured values.

## I. INTRODUCTION

Predicting system performance metrics such as Signal-to-Noise Ratio (SNR), Error Vector Magnitude (EVM) and the waveform quality factor ( $\rho$ ) is usually a difficult task when the signal is processed by a nonlinear amplifier. A high dynamic range receiver and demodulator are required to detect the baseband symbols necessary for calculating waveform quality metrics. It is therefore desirable to accurately estimate these metrics from measurements which do not require a sophisticated digital receiver.

The nonlinear behavior of RF and microwave amplifiers result in in-band (or co-channel) distortion which is manifested as a degradation of SNR and ultimately as a degradation of Bit Error Rate (BER).  $\rho$  and EVM are measures of the fidelity of a digital communication system and are related to in-band distortion and SNR. Characterizing in-band distortion and its relation to the system metrics require the correlated and the uncorrelated components of the output spectrum to be identified. The correlated output component consists of an amplified version of the input waveform with

gain compression/expansion and represents the useful part of the output that leads to correct detection of the received data. On the other hand the uncorrelated part adds to the system interference in a similar way to that of Additive White Gaussian Noise (AWGN). Thus the correlated and the uncorrelated nonlinear output components contribute differently to the degradation of system SNR, EVM,  $\rho$  and ultimately system BER.

In [1] we reported a behavioral modeling technique that enables the effective in-band distortion to be predicted from basic amplifier characteristics without any assumption on signal statistics such as the Gaussian assumption. The technique is based on separating the correlated and uncorrelated components of the output spectrum and hence it allows the in-band distortion to be identified. In this paper we utilize this technique and develop a formulation of in-band distortion and its relation to the most common metrics of system performance; SNR, EVM and  $\rho$ . In addition we develop the relationship among the three metrics. These relationships are verified by direct measurements performed on an IS-95 system using a vector signal analyzer and vector signal generator. Measurement of in-band distortion of a high frequency signal is based on a feed-forward cancellation measurement scheme to remove the correlated component of the output spectrum.

## II. RELATIONSHIP BETWEEN SYSTEM METRICS AND IN-BAND DISTORTION

In order to develop the relationship between the co-channel distortion and system metrics we need to write the output autocorrelation function (which is directly related to the output spectrum) as the sum of uncorrelated components. Using the analysis in [1] the output of a nonlinear amplifier is expressed as a useful component  $\tilde{y}_c(t)$  correlated with the input signal, an uncorrelated distortion component  $\tilde{y}_d(t)$ :

$$\hat{y}(t) = \tilde{y}_c(t) + \tilde{y}_d(t). \quad (1)$$

This work is funded by the National Science Foundation under Grant CCR-0120319 and by the U.S. Army Research Laboratory and the U.S. Army Research Office as a Multi-disciplinary University Research Initiative on Multifunctional Adaptive Radio Radar and Sensors (MARRS) under grant number DAAD19-0101-0496.

The useful part of the signal  $\tilde{y}_c(t)$  consists of the linearly amplified version of the input signal and the correlated part of the spectral regrowth term. The correlated portion of the distortion does not contribute to distortion noise but rather affects the signal level in a manner akin to gain saturation or enhancement of discrete tones. The uncorrelated part of the output  $\tilde{y}_d$  is additive distortion noise and affects system performance in a similar way to AWGN. Thus both the correlated and uncorrelated parts of the output affects the output SNR and BER in different ways. Now, using the orthogonal behavioral model, the output autocorrelation function can now be written as

$$R_{\tilde{y}\tilde{y}}(\tau) = R_{\tilde{y}_c\tilde{y}_c}(\tau) + R_{\tilde{y}_d\tilde{y}_d}(\tau) \quad (2)$$

where

$$R_{\tilde{y}_c\tilde{y}_c}(\tau) = |c_1|^2 R_{u_1 u_1}(\tau)$$

and

$$R_{\tilde{y}_d\tilde{y}_d}(\tau) = \sum_{n=3}^N |c_n|^2 R_{u_n u_n}(\tau).$$

The output Power Spectral Density (PSD) is obtained from the Fourier transform of 2:

$$S_{\tilde{y}\tilde{y}}(f) = S_{\tilde{y}_c\tilde{y}_c}(f) + S_{\tilde{y}_d\tilde{y}_d}(f). \quad (3)$$

The output spectrum is therefore the sum of the spectra of the uncorrelated signal components of the output waveform.

At the receiver, the received signal consists of the amplified transmitted signal and an AWGN component. Therefore, the signal at the receiver can be written in complex envelop form as

$$\tilde{r}(t) = \tilde{y}_c(t) + \tilde{y}_d(t) + \tilde{n}(t) \quad (4)$$

where  $\tilde{n}(t)$  is AWGN component with power spectral density of  $N_0$ . Note that the three output components are now uncorrelated and therefore the uncorrelated output distortion is treated as an additive noise similar to AWGN. The total system noise which affects the output signal quality (and hence system BER) consists of uncorrelated in-band distortion and AWGN as will be seen in the following. In the following we derive the most common measures of in-band distortion using the above analysis.

#### A. Signal-to-Noise Ratio (SNR)

The effective system SNR is defined as the ratio of signal power to total noise power including the power of the in-band distortion terms. It can be expressed in terms

of the PSD's of the uncorrelated output components of (4) as

$$\text{SNR} = \frac{\int_{-B/2}^{B/2} S_{\tilde{y}_c\tilde{y}_c}(f) df}{\int_{-B/2}^{B/2} S_{\tilde{y}_d\tilde{y}_d}(f) df + N_0 B} \quad (5)$$

where  $S_{x_x}(f)$  is the PSD of signal  $x(t)$  and  $B$  is the bandwidth of the input signal. Note that SNR is a function of both the nonlinear distortion and the energy per bit-to-AWGN ratio  $E_b/N_0$ . Evaluating the effective SNR is important to determine the system BER and the system Noise Figure (NF). These parameters are usually estimated assuming a linear AWGN channel however nonlinear distortion increases the system BER for a fixed AWGN power.

#### B. CDMA Waveform Quality Factor ( $\rho$ )

The waveform quality factor is a measure of the correlation between a scaled version of the input and the total in-channel output waveforms. Therefore, using the above formulation, the waveform quality factor is defined as:

$$\begin{aligned} \rho &= \frac{E[\tilde{y}(t)\tilde{y}_c^*(t)]^2}{E[|\tilde{y}(t)|^2]E[|\tilde{y}_c(t)|^2]} \\ &= \frac{\int_{-B/2}^{B/2} S_{\tilde{y}_c\tilde{y}_c}(f) df}{\int_{-B/2}^{B/2} S_{\tilde{y}_c\tilde{y}_c}(f) df + \int_{-B/2}^{B/2} S_{\tilde{y}_d\tilde{y}_d}(f) df + N_0 B} \end{aligned} \quad (6)$$

where the in-band portion of the signals  $y(t)$ ,  $y_c(t)$  and  $y_d(t)$  is used in this expression. Note that  $\rho$  can be directly related to the effective SNR and it measure the fraction of the useful part of the signal at the receiver. Comparing (5) and (6), the relationship between  $\rho$  and SNR can be written as

$$\rho = \frac{\text{SNR}}{\text{SNR} + 1}$$

In an IS-95 system  $\rho$  is usually measured when only the pilot channel is transmitted [2]. In this case, the NBGN assumption of the signal model is not valid and therefore the estimated  $\rho$  using the properties of the Gaussian higher order moments does not lead to an accurate estimation of  $\rho$  which gives the above analysis its importance.

#### C. Error Vector Magnitude (EVM)

Error Vector Magnitude (EVM) is a common figure of merit for system linearity in digital wireless communication standards (including GSM, NADC, IS-95 and WCDMA systems) where a maximum level of EVM is specified. EVM is defined in the context of

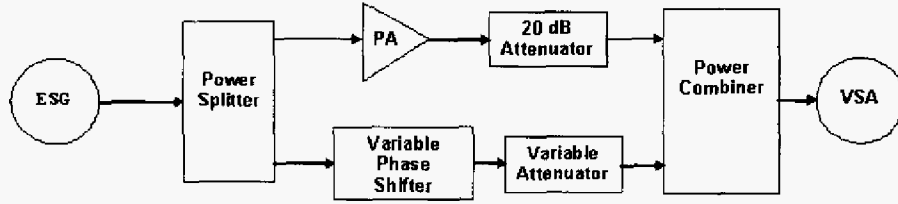


Fig. 1. Feed-forward cancellation measurement setup.

digitally modulated signals where it is a measure of the departure of signals constellation from its ideal reference because of nonlinearity. Nonlinearity results in compression/expansion and rotation of the signal constellation. EVM can be defined using (4) in terms of the signal and noise power as

$$\begin{aligned} \text{EVM} &= \sqrt{\frac{E[\tilde{y}_d^2(t)] + E[\tilde{n}(t)^2]}{E[\tilde{y}_c^2(t)]}} \\ &= \sqrt{\frac{\int_{-B/2}^{B/2} S_{\tilde{y}_d \tilde{y}_d}(f) df + N_0 B}{\int_{-B/2}^{B/2} S_{\tilde{y}_c \tilde{y}_c}(f) df}}. \quad (7) \end{aligned}$$

Using (5) and (6) EVM can be related to SNR and  $\rho$  as follows

$$\text{EVM} = \sqrt{\frac{1}{\text{SNR}}}$$

and

$$\text{EVM} = \sqrt{\frac{1}{\rho} - 1}.$$

Note that EVM and  $\rho$  are directly related to SNR and hence the ability of the receiver to perform reliable detection of the transmitted data.

### III. MEASUREMENTS

The measurements presented here were performed using Agilent E4438C vector signal generator, Agilent E4445A PSA spectrum analyzer and 89600S vector signal analyzer. The in-band distortion is measured using a feed-forward cancellation setup as shown in Fig. 1. The input signal is a forward link IS-95 signal with the pilot only is generated using Agilent ESG 4438C vector signal generator. The signal is split using a power splitter into two branches. The first is amplified by the nonlinear PA under test and the second is used after phase reversal to cancel the linear component of the output. The variable phase shifter and the variable attenuator are used to adjust the linear input level and phase to cancel the linear output of the amplifier. The

resulting output at the power combiner consists of the total uncorrelated distortion (in-band and out-of-band). The in-band distortion is measured as the uncorrelated distortion within the signal bandwidth using an Agilent E4445A PSA spectrum analyzer. Fig. 2 shows measured total output and the uncorrelated distortion spectra. The measured in-band distortion as a function of the output power is shown in Fig. 3(a). The minimum measured in-band distortion (at low power levels) is limited by the finite cancellation that the feed-forward approach provides [3]. This is due to the finite gain and phase matching that can be achieved by the instrument and the measurement setup.

The SNR,  $\rho$  and EVM were estimated from the in-band distortion and verified by directly using a VSA. A measured SNR of 32 dB at small signal (which represents a lower limit of the noise power in the VSA measurements) was included in the estimate of the metrics. Figs 4 (b), (c) and (d) show a good agreement between measured and estimated values.

### IV. CONCLUSION

A technique to directly relate system metrics to nonlinear distortion has been developed and verified. SNR, EVM and  $\rho$  were estimated from in-band distortion measured using feed-forward cancellation. The estimated metrics are in excellent agreement with direct measurements of system metrics using a VSA. The simplicity of the measurement enables the metrics to be predicted using simple lab equipment.

### REFERENCES

- [1] K. M. Gharaibeh and M. B. Steer, "Performance Analysis of Direct Sequence Spread Spectrum (DS-SS) CDMA System With Amplifier Nonlinearities." *IEEE Radio and Wireless Conference, RAWCON 2004*, Sep. 2004.
- [2] V. Aparin, "Analysis of CDMA signal spectral regrowth and waveform quality." *IEEE Trans. Microwave Theory Techn.*, Vol. 49, pp. 2306-2314, Dec. 2001.
- [3] P. B. Kenington, *High Linearity Amplifier Design*, Massachusetts: Artech House Inc., 2000.

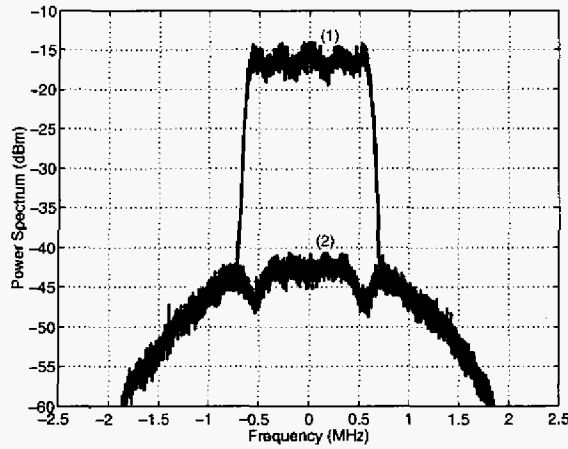
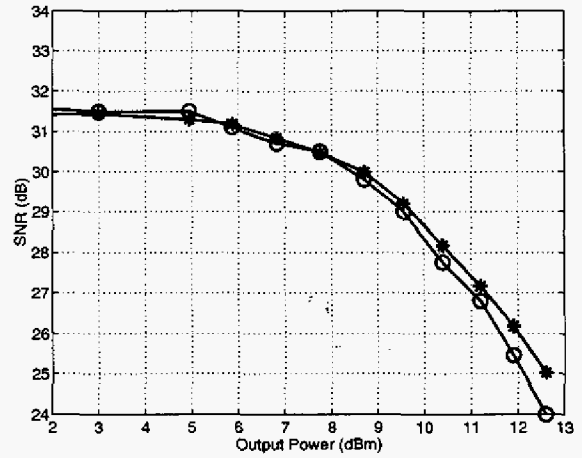


Fig. 2. (a) Measured spectrum: (1) total output spectrum and (2) in-band distortion (output of the feed-forward loop).



(a)

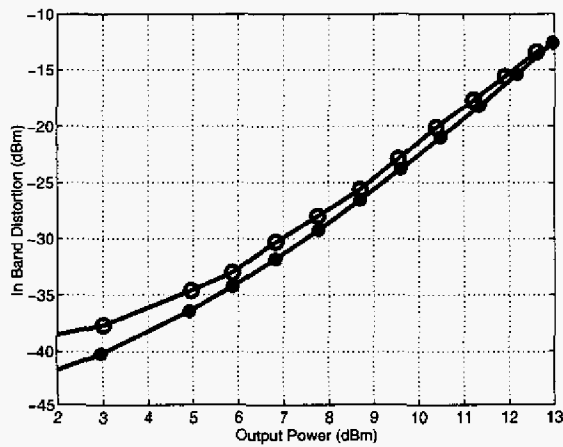
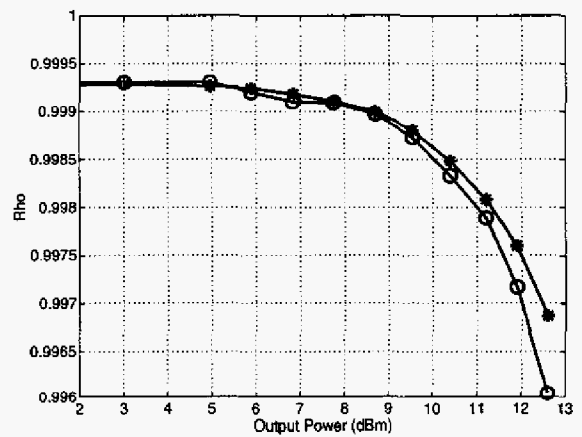
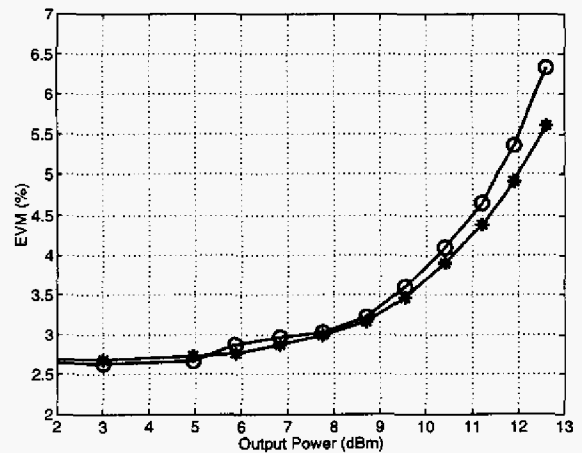


Fig. 3. In-band distortion power;  $\circ$ : measured; and  $*$ : simulated.



(b)

- [4] K. Gard, H. Gutierrez, M. B. Steer, "Characterization of spectral regrowth in microwave amplifiers based on the nonlinear transformation of a complex Gaussian process," *IEEE Trans. Microwave Theory Techn.*, Vol. 47, pp. 1059–1069, July 1999.
- [5] N. Blachman, "The uncorrelated output components of a non-linearity," *IEEE Trans. Inf. Theory*, Vol. 14, pp. 250–255, March 1968.
- [6] P.M. Lavrador, N.B. de Carvalho and J.C. Pedro, "Evaluation of signal-to-noise and distortion ratio degradation in nonlinear systems," *IEEE Trans. Microwave Theory Techn.*, Vol. 49, pp. 813–822, March 2004.
- [7] J. S. Bendat, *Nonlinear System Analysis and Identification*, John Wiley and Sons, NY 1990.
- [8] T. S. Rappaport, *Wireless Communications: Principles and Practice*, New Jersey: Prentice Hall Inc., 1996.
- [9] M. Jeruchim, P. Balaban and S. Shanmugan, *Simulation of Communication Systems*, New York: Kluwer Academic/Plenum Publishers, 2000.



(c)

Fig. 4. System metrics: (a) SNR, (b)  $\rho$  and (c) EVM vs. output power;  $\circ$ : measured; and  $*$ : estimated using measured in-band distortion.

# EVM Calculation for Broadband Modulated Signals\*

Michael D. McKinley<sup>1</sup>, Kate A. Remley<sup>1</sup>, Maciej Myslinski<sup>2</sup>, J. Stevenson Kenney<sup>3</sup>, Dominique Schreurs<sup>2</sup>, Bart Nauwelaers<sup>2</sup>

<sup>1</sup>Electromagnetics Division, National Institute of Standards and Technology  
mckinm, remley@boulder.nist.gov,

<sup>2</sup>ESAT-TELEMIC, Katholieke Universiteit Leuven, Belgium

Maciej.Myslinski, Dominique.Schreurs, Bart.Nauwealears@esat.kuleuven.ac.be

<sup>3</sup>Georgia Institute of Technology, jskenney@ece.gatech.edu

**Abstract:** We present a normalization that facilitates calculation of error vector magnitude (EVM) from measurements. We derive the definition of EVM for a common industry standard from a more basic equation. We compare EVM for various modulation types for a given average symbol power under simple distortion conditions.

**Keywords:** Digital Modulation; Error Vector Magnitude; Vector Signal Analyzer; Wireless Telecommunications.

## I. Introduction

Error vector magnitude (EVM) is a common figure of merit for assessing the quality of digitally modulated telecommunication signals. EVM expresses the difference between the expected complex voltage value of a demodulated symbol and the value of the actual received symbol. While another common figure of merit, bit error rate, gives a “go,” “no-go” level of system characterization, EVM can be more useful to the microwave engineer because it contains information about both amplitude and phase errors in the signal [1], [2]. This additional information can allow a more complete picture of the channel distortion and is more closely related to the physics of the system.

Because of the potential for mixing of in-band frequency components, EVM is often used to characterize signals that use broadband schemes for transmitting large amounts of data at relatively high speeds. The most common of these schemes at 5 GHz is known as orthogonal frequency-division multiplexing (OFDM), as specified by the IEEE 802.11a<sup>TM</sup>-1999 standard [2], [3]. OFDM is used in wireless local-area networks (WLANs), in the Dedicated Short-Range Communication (DSRC) systems for tracking and observing loads in commercial vehicles [4], and in the recently opened public-safety band at 4.9 GHz.

The IEEE 802.11a<sup>TM</sup>-1999 standard specifies use of several different OFDM modulation types (i.e., binary phase-shift keying (BPSK), quadrature phase-shift keying (QPSK), 16-symbol quadrature amplitude modulation (16QAM), 64-symbol quadrature amplitude modulation (64QAM), etc.) that may be used in adjacent bursts. Even within one burst more than one modulation format may be used since the four pilot subcarriers are always transmitted using BPSK. This motivates the use of normalization, to calculate EVM easily and to enable direct comparison of EVM for a given average power level per symbol between modulation types. Such normalization is implicit in the IEEE 802.11a<sup>TM</sup>-1999 standard and is the focus of this paper.

We first briefly introduce a common representation of demodulated symbols for the digital modulation types used in the IEEE 802.11a<sup>TM</sup>-1999 standard. Following this, we derive a normalization that lets us find EVM by comparing an ideal symbol value to one that is measured. This direct calculation of EVM means that, on a normalized plot, the magnitude of the error vector for each symbol equals the symbol's EVM. The normalization also aids the comparison of

---

\* Work of the United States government, not subject to U.S. copyright

EVM for various modulation types for a given average symbol power. Finally, we compare EVM for the different modulation types used in the IEEE 802.11a<sup>TM</sup>-1999 standard.

## II. Normalization to Enable Direct EVM Calculation and Comparison

EVM measurements are often performed on vector signal analyzers (VSAs), real-time analyzers or other instruments that capture a time record and internally perform a Fast Fourier Transform (FFT) to enable frequency-domain analysis. Calculation of EVM is often accomplished through software internal to these instruments. Signals are downconverted and demodulated before EVM calculations are made. As discussed above, to calculate and compare EVM efficiently for different modulation types, some normalization is typically carried out.

### A. Constellation Diagrams and EVM

To aid in the visualizing of demodulated signals, constellation diagrams are often used to represent digital bits in terms of symbols. In a sense, constellation diagrams are the bridge between digital and analog representations of a data stream. A constellation diagram is a plot of symbols where each symbol represents one or more bits (depending on the modulation type)—the digital aspect. It is also a plot where each symbol is represented by a unique magnitude and phase—the analog aspect.

Figure 1 shows three constellation diagrams for 16QAM, which has 16 symbols that modulate the RF carrier in both magnitude and phase. In each case,  $I$  and  $Q$  represent the in-phase ( $0^\circ$  relative phase) and quadrature ( $90^\circ$  relative phase) values of each symbol. This gives each symbol a resulting magnitude and phase. Figure 1(a) represents a measured set of symbols. The  $V_I$  and  $V_Q$  axes give, respectively, the measured in-phase and quadrature ( $90^\circ$  relative phase) voltage levels for a complex voltage representation. Scattered dots on this diagram represent the effect of small errors in the measured symbols. Figure 1(b) represents the ideal constellation described below. The units of the in-phase and quadrature axes are dimensionless integers and are represented by  $C_I$  and  $C_Q$ , respectively.

To efficiently calculate EVM, the diagrams in Figs. 1(a) and 1(b) are scaled to form the normalized (dimensionless) constellation diagram in Fig. 1(c). The in-phase ( $S_I$ ) and quadrature ( $S_Q$ ) axes are similar to the real and imaginary axes used in complex voltage representations. We derive a scaling for these constellations in this section.

To enable the normalization, we assume a uniform distribution of the transmitted symbols onto the constellation. This means that the transmitted symbols have an equal probability of visiting each location on the constellation and that the number of symbols transmitted is a multiple of the number of unique symbols in a constellation. We also assume that before normalization occurs the receiver has derotated the received symbols so that they are aligned in the constellation. Systematic rotation of symbols can occur, for example, when there is a difference between the sampling frequency (typically set by the center frequency) and that of a given subcarrier. In this case, the rotation is greatest on the outermost subcarriers and enlarges with each subsequent OFDM symbol received. Due to the commonality of the problem, all OFDM receivers have derotation operations built into them.

**Ideal Constellation.** Constellation diagrams that show the ideal placement of symbols for a given modulation type are often represented by symbols at integer levels. We saw this in Fig. 1(b), where the constellation diagram for 16QAM was shown.

Furthermore, the number of levels along either an in-phase or quadrature axis for an ideal constellation is

$$n = \sqrt{N} \quad . \quad (1)$$

For example, since  $N = 16$  for 16QAM, there are four symbol levels ( $n = 4$ ) for both the in-phase and quadrature axes. The integer coordinates of the ideal constellation points for each symbol are

$$C_{\text{ideal},pq} = C_{L,\text{ideal},pq} + jC_{Q,\text{ideal},pq} = (2p - 1 - n) + j(2q - 1 - n) \quad , \quad (2)$$

where the integers  $p$  and  $q$  satisfy  $1 \leq p \leq n$ ,  $1 \leq q \leq n$ , and the integer  $n$  is defined in (1). From (2), we can obtain what we refer to here as the “ideal constellation diagram,” Fig. 1(b), for any of the common digital modulation types.

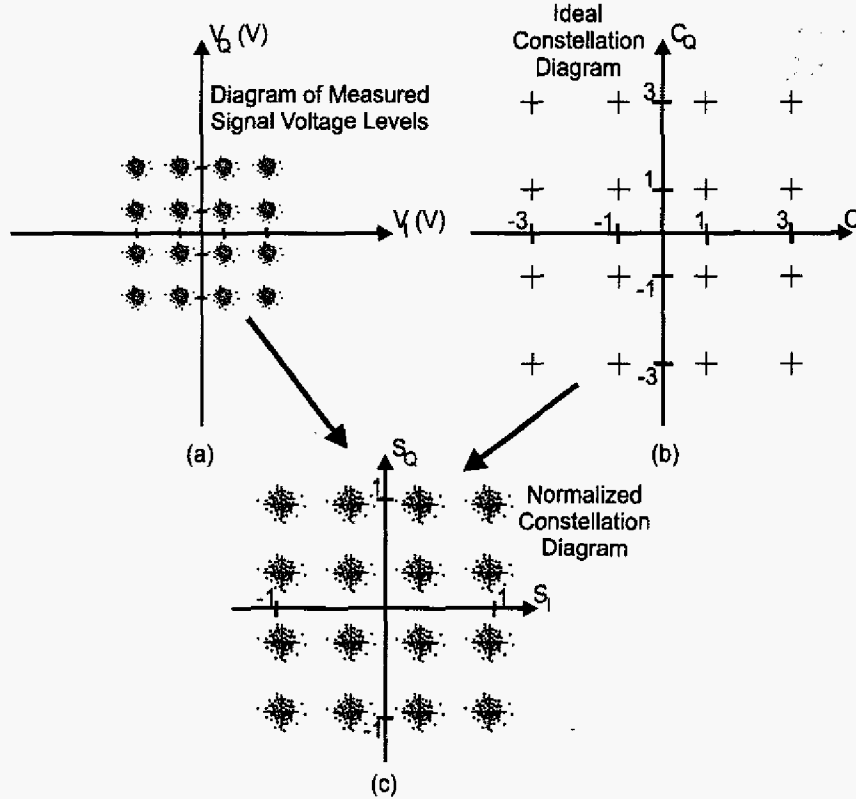


**Figure 1:** Graphs of (a) measured symbols, (b) the ideal constellation diagram, and (c) a normalized space that facilitates calculation of EVM.

**Normalized Constellation.** Figure 2 again shows the normalized constellation diagram representation from Fig. 1(c). Our normalization is derived such that the mean-square amplitude of all possible symbols in the constellation is one, as discussed below. Figure 2 also shows the error vector for one measured symbol. In this special case with only one measured symbol, the magnitude of this small vector equals the EVM. If there were more symbols acquired than just this one, the EVM would equal the sum of the magnitudes of the error vectors for all of the measured symbols divided by the total number of measured symbols.

Thus, when symbols have been normalized, EVM is defined as the root-mean-square (RMS) value of the difference between a collection of measured symbols and ideal symbols (also RMS quantities). These differences are averaged over a given, typically large, number of symbols and are often shown as a percent of the average power per symbol of the constellation.

As given in (2) of [5], EVM can be expressed mathematically as

$$EVM_{\text{RMS}} = \left[ \frac{\frac{1}{N} \sum_{r=1}^N |S_{\text{ideal},r} - S_{\text{meas},r}|^2}{\frac{1}{N} \sum_{r=1}^N |S_{\text{ideal},r}|^2} \right]^{\frac{1}{2}}, \quad (3)$$

where  $S_{\text{meas},r}$  is the normalized  $r^{\text{th}}$  symbol in a stream of measured symbols,  $S_{\text{ideal},r}$  is the ideal normalized constellation point for the  $r^{\text{th}}$  symbol, and  $N$  is the number of unique symbols in the constellation.<sup>1</sup>

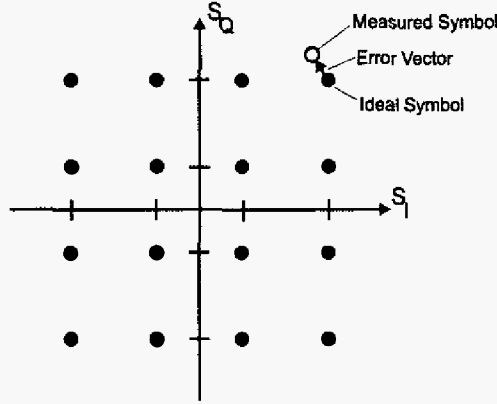


Figure 2: Normalized constellation diagram for 16QAM [1].

### B. Normalizations of the measured and ideal representations

To find EVM, we must compare the ideal symbol values from the ideal constellation diagram to the arbitrary voltage values that we measure. One way to enable this comparison is to normalize both the measured and ideal symbols, as illustrated in Fig. 1. We describe this procedure below.

**Measured Case.** For the measured case, one method for accomplishing this normalization is to divide the power in each symbol,  $P_{V,\text{symbol}}$ , by the average symbol power calculated over all symbols in the constellation, to obtain  $P_{S,\text{symbol}}$ :

$$P_{S,\text{symbol}} = \frac{P_{V,\text{symbol}}}{P_V / T}, \quad (4)$$

where  $P_V$ , the total power of a measured constellation having  $T$  symbols, is

$$P_V = \sum_{r=1}^T \left[ (V_{I,\text{meas},r})^2 + (V_{Q,\text{meas},r})^2 \right] \text{ (W)}, \quad (5)$$

where  $V_{I \text{ or } Q,\text{meas},r}$  is the RMS voltage level of the in-phase and quadrature components of the measured symbols and  $T$  is typically  $\gg N$ .

<sup>1</sup> Thus,  $N=16$  for the 16QAM case. For the measured case, averaging is typically carried out. Thus,  $N$  should be replaced with  $T$  = total number of symbols measured. Typically,  $T \gg N$ .

From (4), we see that  $P_{S,\text{symbol}}$  is dimensionless. The average of all  $P_{S,\text{symbol}}$ 's in the normalized constellation will be equal to one. For example, the normalized constellation for 16QAM is given in Fig. 3.

To calculate EVM, we must represent this normalization in terms of voltage. We identify a normalization factor  $|A_{\text{meas}}|$  from (4) as

$$|A_{\text{meas}}| = \sqrt{\frac{1}{P_V/T}} \quad (6)$$

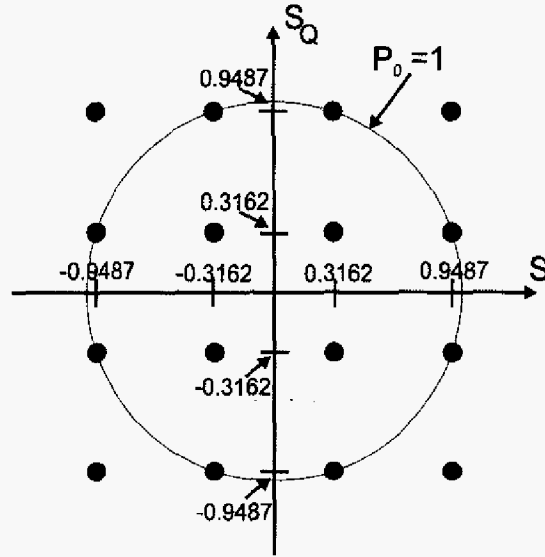


Figure 3: Normalized constellation diagram.

**Ideal Case.** For the ideal case, we carry out the normalization in an integer space rather than a voltage space. However, a similar procedure can be used for the integer space if we use  $N$  instead of  $T$  where  $N$  is the number of unique symbols in a constellation (e.g., 4 for QPSK or 16 for 16QAM). In this case,  $P_C$  does not represent the total power in a constellation as does  $P_V$ , but is rather the sum of the squares of the amplitudes of all symbols:

$$P_C = \sum_{p=1}^n \left[ \sum_{q=1}^n (C_{I,\text{ideal},pq}^2 + C_{Q,\text{ideal},pq}^2) \right] \quad (7)$$

Here,  $C_{I,\text{ideal},pq}$  and  $C_{Q,\text{ideal},pq}$  are, respectively, the real (in-phase) and imaginary (quadrature) integer values corresponding to each symbol, and  $n$  is defined in (1). Note that for the ideal, integer-based constellation diagram (Fig. 1(b)),  $P_C$  can also be found by substituting the values in (2) for  $C_I$  and  $C_Q$ :

$$P_C = \sum_{p=1}^n \left[ \sum_{q=1}^n ((2p-1-n)^2 + (2q-1-n)^2) \right] \quad (8)$$

Similar to (6), the normalization scaling factor for ideal symbols,  $|A_{\text{ideal}}|$ , is written as

$$|A_{\text{ideal}}| = \sqrt{\frac{1}{P_C / N}} \quad (9)$$

**Normalized EVM.** From (6) and (9), EVM can be represented as

$$EVM_{\text{RMS}} = \left[ \frac{\frac{1}{T} \sum_{r=1}^T \left( |(V_{I,\text{meas},r}) \cdot |A_{\text{meas}}| - (C_{I,\text{ideal},r}) \cdot |A_{\text{ideal}}|^2 + |(V_{Q,\text{meas},r}) \cdot |A_{\text{meas}}| - (C_{Q,\text{ideal},r}) \cdot |A_{\text{ideal}}|^2 \right)}{P_{S,\text{avg}}} \right]^{\frac{1}{2}}, \quad (10)$$

where

$$P_{S,\text{avg}} = \frac{1}{N} \sum_{p=1}^n \left[ \sum_{q=1}^n \left( (2p-1-n)^2 |A_{\text{ideal}}|^2 + (2q-1-n)^2 |A_{\text{ideal}}|^2 \right) \right]. \quad (11)$$

In (11),  $P_{S,\text{avg}}$  is the normalized mean-square amplitude of the symbols in the constellation. It is always equal to one, and is the same as  $P_0$  in [1].  $V_{I\text{or}Q,\text{meas},r}$  and  $C_{I\text{or}Q,\text{ideal},r}$  are the unnormalized voltages and integer values, respectively, for the  $r^{\text{th}}$  symbol for the measured and ideal in-phase and quadrature components. The quantities  $A_{\text{meas}}$  and  $A_{\text{ideal}}$  refer, respectively, to the normalization factors in (6) and (9) calculated for the measured and ideal constellations. The limit  $T$  encompasses all measured symbols and satisfies the relation  $T \gg N$ .

### C. EVM and the IEEE 802.11a<sup>TM</sup>-1999 standard

From the representation of (10), we can easily derive the expression for EVM in the IEEE 802.11a<sup>TM</sup>-1999 standard. We first identify the normalized voltages in terms of  $I$  and  $Q$  to get

$$EVM_{\text{RMS}} = \left[ \frac{\frac{1}{T} \sum_{r=1}^T \left( |I_r - I_{0,r}|^2 + |Q_r - Q_{0,r}|^2 \right)}{P_0} \right]^{\frac{1}{2}}, \quad (12)$$

where  $I_r = (V_{I,\text{meas},r}) \cdot |A_{\text{meas}}|$ ,  $Q_r = (V_{Q,\text{meas},r}) \cdot |A_{\text{meas}}|$ ,  $I_{0,r} = (C_{I,\text{ideal},r}) \cdot |A_{\text{ideal}}|$ , and  $Q_{0,r} = (C_{Q,\text{ideal},r}) \cdot |A_{\text{ideal}}|$ .

The IEEE 802.11a<sup>TM</sup>-1999 standard includes some of the specifics of the multiplexing types: the subcarriers (52 total), the length of the packets (i.e., the number of symbols in a packet),  $L_p$ , and the number of frames received,  $N_f$ . This gives us the equation given in [1]:

$$EVM_{\text{RMS}} = \frac{\sum_{i=1}^{N_f} \left[ \frac{\sum_{j=1}^{L_p} \left\{ \sum_{k=1}^{52} \left[ |I(i,j,k) - I_0(i,j,k)|^2 + |Q(i,j,k) - Q_0(i,j,k)|^2 \right] \right\}}{52 \cdot L_p \cdot P_0} \right]^{\frac{1}{2}}}{N_f}. \quad (13)$$

With the normalization derived above applied in (13), we are able to compare EVM across subcarriers, packets and frames for bursts with different modulation types as long as the average

power per symbol and the center frequency of the signal are consistent. The ability to directly compare EVM for different modulation types is important since the IEEE standard specifies use of BPSK modulation for the four pilot subcarriers, while the 48 remaining data subcarriers may utilize a different modulation scheme. By including all 52 subcarriers, (13) is able to include, for example, errors on the composite signal due to frequency-response effects across its wide bandwidth or frequency-dependent distortion effects due to nonlinear amplification.

### III. EVM for Different Modulation Types in Different Environments

We used two measurement set-ups to test the effects of simple channel distortion on EVM across different modulation types. We generated modulated signals in the IEEE 802.11a<sup>TM</sup>-1999 standard at 5 GHz using a vector signal generator (VSG). The 5 GHz signals were downconverted externally and sent to our vector signal analyzer. One test set-up was designed to represent a low-distortion, best-case scenario for our instrumentation. In this case, we fed the output of our VSG directly to the frequency converter through a cable. This set-up is the same as that shown in Fig. 4 but with the tuner and splitter/combiner replaced with one cable.

For the second test, we intentionally introduced distortion to increase EVM. We split the signal from the VSG into two branches, as shown in Fig. 4. We fed one branch through a cable to an impedance tuner that introduced some phase shift and distortion of the modulated signal, while the other branch was fed through a cable. The two branches were then recombined and downconverted to the frequency range of our VSA.

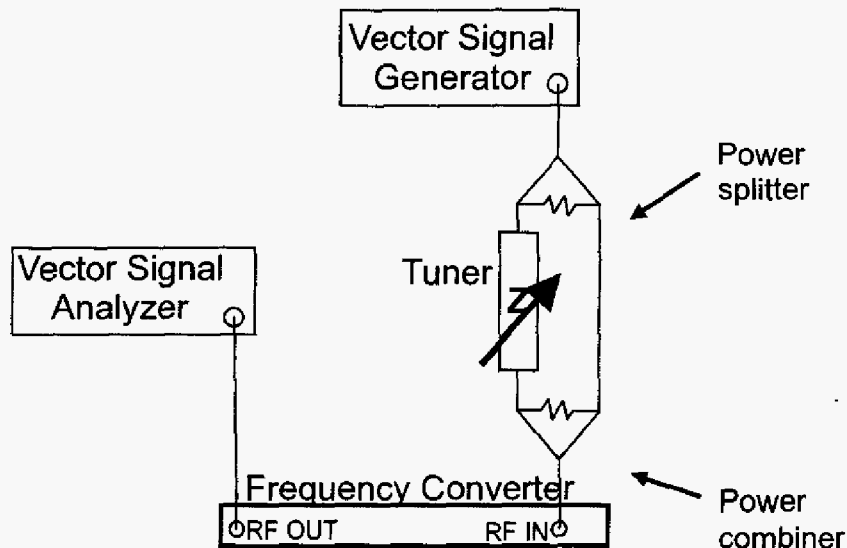
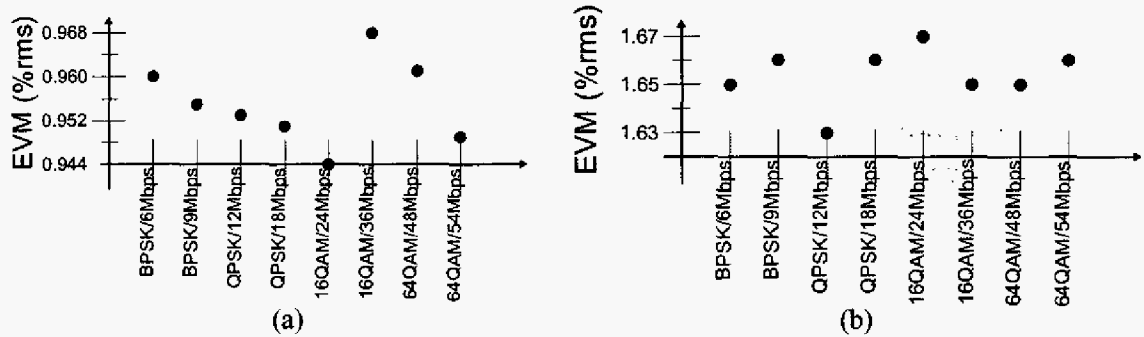


Figure 4: Higher-distortion test set-up for measuring EVM.

We measured EVM using the VSA for all of the modulation types used in the IEEE 802.11a<sup>TM</sup>-1999 standard. We used a commercial package to calculate the EVM for the composite signal, as in (13). The specification for EVM in the data sheet of this commercial package is  $<1\%$ . Our EVM for the low-distortion case was within this range, as shown in Fig. 5(a). For each measurement of the low-distortion case, we received an average symbol power of  $\sim 1.77 \mu\text{W}$  ( $9.41 \pm 0.04 \text{ mV}_{\text{rms}}$  across  $50 \Omega$ ) with all 48 data subcarriers set to the same modulation format.

Results for the higher-distortion set-up are shown in Fig. 5(b). For each measurement in this set-up, we measured an average symbol power of  $\sim 28.5 \text{ nW}$  ( $1.194 \pm 0.006 \text{ mV}_{\text{rms}}$  across  $50 \Omega$ ) with all 48 data subcarriers set to the same modulation format. The relatively low increase in

overall EVM for the higher-distortion case can be attributed to a cyclic prefix that is included in the IEEE 802.11a<sup>TM</sup>-1999 standard to minimize the effects of multipath distortion. The cyclic prefix is obtained by copying the rear part of a burst and attaching it to the front. By allowing any carry-over energy due to multipath effects or intersymbol interference from a previous burst to fall into the cyclic prefix and not into the main signal, the effects of these types of interference on EVM are minimized.



**Figure 5:** EVM for the modulation types used in the IEEE 802.11a<sup>TM</sup>-1999 standard for (a) a low-distortion case and (b) a higher-distortion case utilizing a two-path channel and a tuner.

Our measurements demonstrate that the normalization defined by (10) does enable direct comparison of EVM for the different modulation types for a given average symbol power. While EVM did change between the two setups, little change occurred between the various modulation types. The EVM values in Fig. 5 for both the low- and high-distortion cases varied by less than 0.05 %. On a scale showing 0-1 % EVM or 0-2 % EVM for the low and high EVM cases, respectively, the plotted points resemble a flat line.

#### IV. Discussion and Conclusions

We derived a normalization for measured symbols and constellation diagrams that enables ready calculation of EVM. This involved multiplying the in-phase and quadrature voltages for each measured or ideal symbol in the constellation by a factor that yields a mean-square symbol amplitude with a value of one. We showed the equivalence of our normalized representation of EVM and the EVM in the IEEE 802.11a<sup>TM</sup>-1999 standard. This demonstration went from a simple mathematical representation to one that takes frames, packet length and all 52 subcarriers into account. We compared measurements of EVM for different modulation types in the IEEE 802.11a<sup>TM</sup>-1999 standard for simple low- and high-distortion scenarios.

**Acknowledgements:** The authors are grateful for help and suggestions on the manuscript from Dylan Williams, Joe Tauritz, John Meister, Timothy J. Peters, and Bob Cutler.

#### References:

- [1] IEEE Standard for Wireless LAN Medium Access Control (MAC) and Physical Layer (PHY) Specifications: High-Speed Physical Layer in the 5 GHz Band, IEEE Standard 802.11a<sup>TM</sup>-1999.
- [2] IEEE Standard for Wireless LAN Medium Access Control (MAC) and Physical Layer (PHY) Specifications: Higher-Speed Physical Layer Extension in the 2.4 GHz Band, IEEE Standard 802.11b-1999.
- [3] This standard is identified solely for completeness of description, but such identification does not constitute an endorsement by the National Institute of Standards and Technology. Other products may work as well or better.
- [4] <http://www.leearmstrong.com/DSRC/DSRCHomeset.htm>
- [5] S. Forestier, P. Bouysse, R. Quere, A. Mallet, J.-M. Nebus, and L. Lapiere, "Joint optimization of the power-added efficiency and the error-vector measurement of 20-GHz pHEMT amplifier through a new dynamic bias-control method," *IEEE Trans. Microwave Theory and Tech*, vol. 52, no.4, pp. 1132-1140, Apr. 2004.

# Dynamic Complex IMD Measurement System

Basim Noori, Khan Salam and Mohammed Sajid  
REMEC Mobile Wireless  
Folsom

## I. Abstract

A method for measuring the complex distortion products generated through an active device-under-test as a function of input RF power is presented in this paper. The main motivation behind this exercise is to give the PA designer a quick understanding of the behavior of the Device-Under-Test (DUT) over a range of bias points, drain voltage, etc., without resorting to the traditional lengthy methods of gathering the output data of each power step then plotting the result in a spreadsheet.

In addition, the complex amplitude and phase (or real and imaginary) components of the IMD products in a cascaded line-up of devices or individual stages may be measured.

The system employs a simple two-tone configuration with no additional special components such as mixers or down-converters. The tone separation is dictated by the passive components and the upper frequency limit of the instruments.

## I. Introduction

In recent years, a concerted effort has taken place to further the understanding of complex distortion product behavior generated by non-linear devices in general and by power

electronics in particular. The study conducted by *de Carvalho & Pedro* [1,2,3,4] provided the academics and designers alike an in-depth understanding of the relationship between IMD products, ACPR and the asymmetry associated with these products. Equally, *Vuolevi & Rahkonen* [5], derived a relationship between electrical memory effects and bias circuit induced IMD asymmetry.

The method described in this document is not intended to substitute the elaborate method described by *Vuolevi, Rahkonen and Manninen* [6], for measuring the IMD phase and magnitude relative to the carrier. Instead, this versatile method is targeted to present the designers with a fast display of the behavior of the complex IM products of a single device or a complete PA line-up, thus enabling them the optimization of the device line up quickly and efficiently. One of the laborious tasks of any designer is the point-by-point measurement of IM sidebands as a function of input or output power. Typically, the measurement is repeated for several bias points and drain (or collector) voltages. One set of measurements over a typical 15dB input power dynamic range takes around 5-10 minutes depending on the user. Using the method described in this paper, IMD magnitude, phase, and vector data can be obtained within seconds per IMD product. The system may be operated manually or automatically and may also be easily integrated with a Load-Pull system.

## II. System description

Figure 1 below, shows the basic building blocks of the system. The constituent elements are:

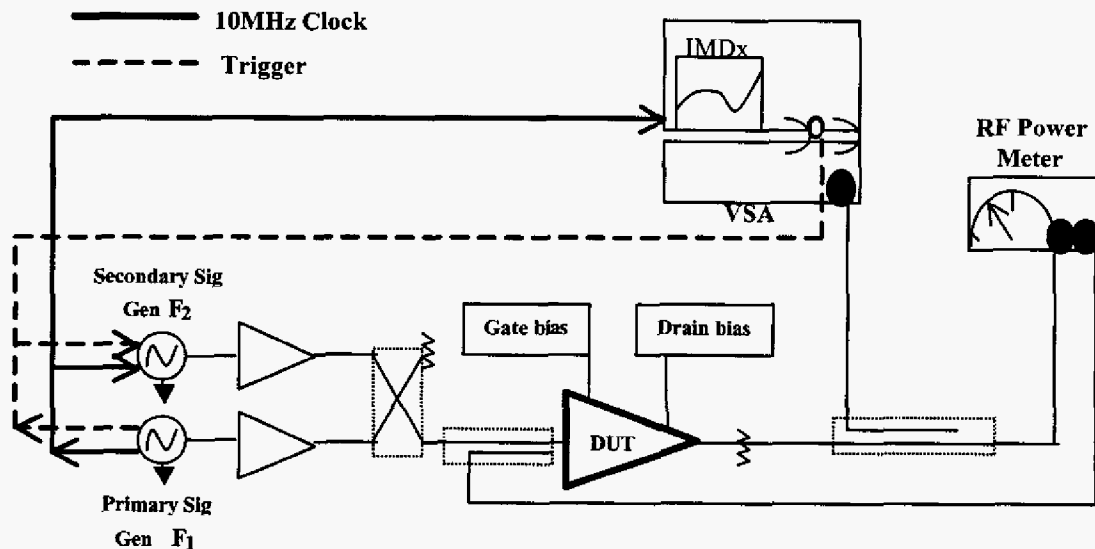


Figure 1 IMD Measurement System Block Diagram

1. Two RF signal sources with external trigger and sweep capability. One ESG with a multi-tone option may be used to replace a 2-ESG setup
2. Two linear bench amplifiers
3. An RF power meter
4. A vector signal analyzer for complex parameter measurements. Or any standard Spectrum Analyzer with triggering capability for magnitude measurements only

A complete set-up and operation guide is presented in the appendix attached. Once the system is triggered, the complex components of each carrier and their corresponding distortion products may be displayed as a function of input power.

Let us examine the plot below, figure 2 shows the swept magnitude response of an LDMOS transistor biased in a typical Class-AB operation. The VSA is set in the Vector mode and the measurements take place in the time domain. That is the reason why the x-axis displays time units rather than logarithmic power units. However, although the VSA display is in time units, it can be easily correlated and converted to the power domain. Simply read the input power meter and normalize the value to the beginning and end of the x-axis on the VSA. For example, if the total carrier input power is 0dBm and the swept range is 15dB, then the end of the x-axis of the SA is 0dBm with a x-scale of 1.5dB/div. Normalizing the scale to the output power is not recommended because the display will not be correlated to gain expansion and compression

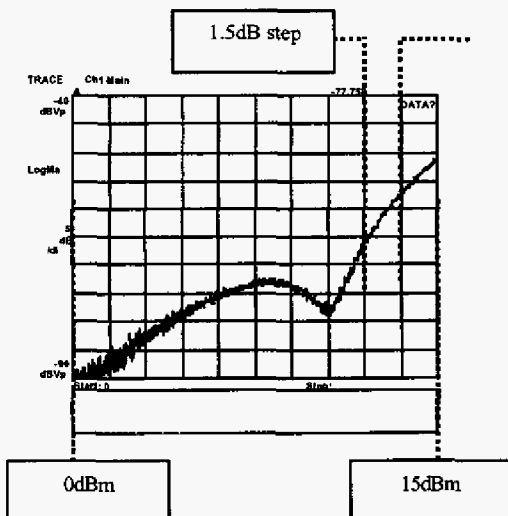


Figure 2 IMD3 Magnitude Response

and non-linear behavior of the DUT, thus compromising the accuracy of the measurement setup. Therefore, displaying the waveform vs. input power is more accurate in this particular set-up.

The phase response of the IMD product clearly adds another dimension when characterizing distortion products. The y-axis of figure 3, depicts the unwrapped phase of an IMD product as a function of input power. Notice that at the same marker point where the notch occurs in the magnitude plot above, the phase is changing dramatically. The phase response is fairly linear for approximately the first 9 dB of the measurement and then goes through a dramatic reversal. The marker below is located exactly at the phase reversal point of the of IM vector. The point of inflection coincides with the nulling observed in the magnitude plot as the vector

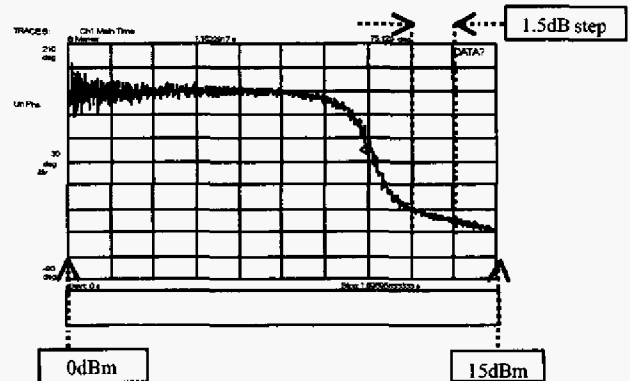


Figure 3 IMD3 Phase Response

passes through the origin. This observation does appeal to our intuition of non-linear behavior and can be shown analytically.

The x-axis of the phase response of the IMD product may be viewed in a similar fashion to the x-axis of the magnitude plot above; the maximum value of the axis is normalized to the maximum input power value.

The magnitude and phase components of the IMD3 product may be re-composed into their basic vector element. In figure 4 plot below, the magnitude, phase and vector plots are overlaid and the markers coupled. The trajectory of the vector traverses 9dB after the onset of the power sweep. In fact, the reversal coincides with the plateau of the magnitude plot, while the notch in the magnitude and phase reversal coincide with the vector passing close to the origin. Note that

the maximum value of the vector trace is normalized to the same maximum value of the phase and magnitude traces as shown in figures 2 & 3 above.

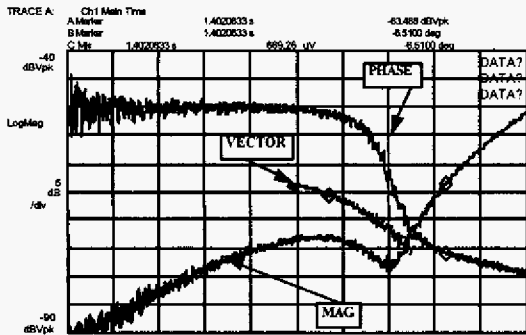


Figure 4 IMD3 Magnitude, Phase and Vector Plots

On the other side of the bias spectrum, the behavior of a class-A power transistor is seen below, with a smooth, almost perfect, 3:1 magnitude response and a transition-free phase response. The vector trajectory in this case has a monotonic outward path.

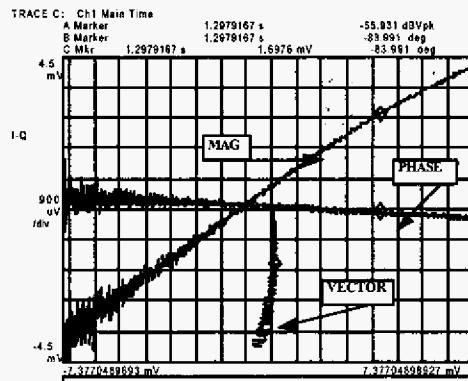


Figure 6 IMD3 Magnitude, Phase and Vector Response of a Class-A Amplifier

### III. System Applications

#### A. Measuring different classes of operation

The behavior of the amplifier under different bias conditions may be studied with relative ease. Below the characteristic "Notch" in the magnitude response can be seen as well as the sharp transition in the unwrapped phase. Here, the vector plot shows a reversal of its trajectory through the origin causing a complete nulling of the IM3 magnitude and a sharp reversal in its phase response.

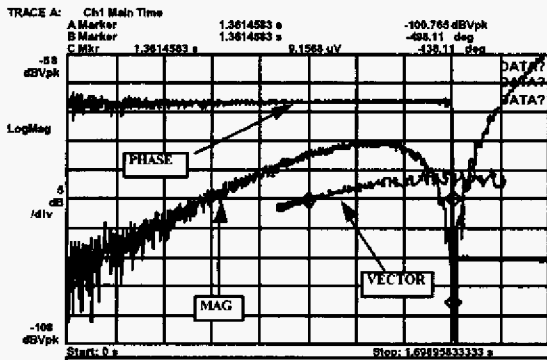


Figure 5 IMD3 Magnitude, Phase and Vector Response of an under-biased Class-AB Amplifier

#### B. Upper/Lower sideband measurement

One of the expanded uses of this system is the study of the frequency dependency of the IMD behaviour as a function of tone spacing; below is an example of the asymmetric response of the IM3 components. The phase and magnitude behaviour of the lower and upper component can be seen as different. The separation of the tones may be increased to determine the modulation bandwidth of the entire circuit.

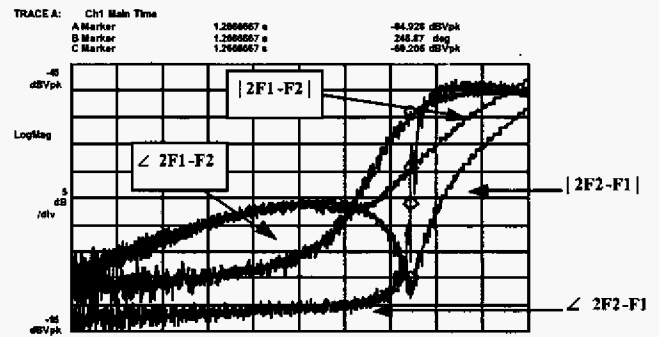
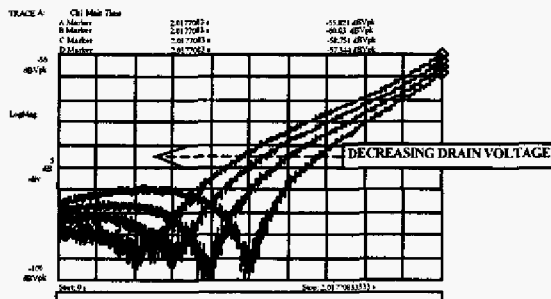


Figure 7 Magnitude and Phase Responses of the upper and lower IMD3 sidebands

### C. Drain Voltage Optimization

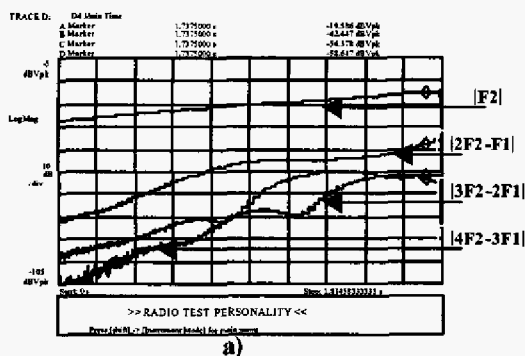
One of the techniques PA designers adopt is the peak power optimization of a particular device through drain voltage manipulation. This system examines the distortion product "Notch" as a function of drain voltage. Figure 8 depicts the 3<sup>rd</sup> order distortion profile of a class-AB amplifier as a function of input power and drain voltage.



**Figure 8** Class AB LDMOS Amplifier "Notch" Optimization Of  $|2F_2-F_1|$ . (Measurement Time Approx. 45 Sec.)

### D. Linearization examination

One of the major benefits of this system is its ability to examine the behavior of several IMD products over a wide dynamic range. As an example, figure 9 depicts the cancellation capability of a pre-distortion system and it's capability to null single or multiple distortion products. Three distortion products are depicted on the same plot, namely, 3<sup>rd</sup>, 5<sup>th</sup>, and 7<sup>th</sup>. The behavior of the overall system is seen to reduce



the IMD products over the lower portion of the

power sweep while increasing them towards the upper portion.

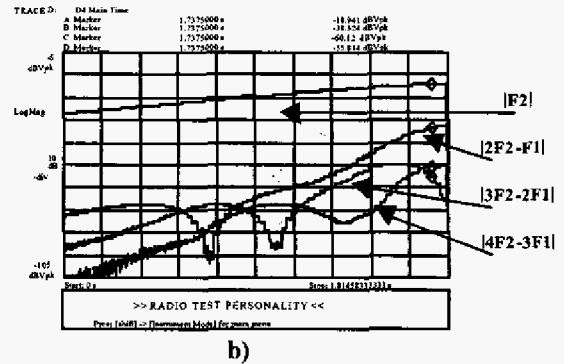


**Figure 9** IMD Optimization For A Predistortion System. a) before ,and b) after

### Conclusion:

A useful system is proposed that enables the study of complex components of the intermodulation distortion behaviour of a DUT, in this case a power amplifier. The ability to quickly display magnitude, phase and vector sweeps vs. input power were shown. The behaviour of different bias conditions were also studied as well as asymmetry of the lower/upper IMD products.

This method enables the conversion of the independent variable on the x-axis from time swept data to any other independent variable such as power, gate or drain voltage, frequency, etc., thereby enabling the measurement of numerous dynamically swept waveforms which were traditionally measured using static step-by-step methods.

### Acknowledgments:

The authors would like to thank Mar Caballero of REMEC, Inc. for his measurements and helpful hints.

### References:

[1] N. Carvalho and J. Pedro, "Large and Small Signal IMD Behavior of Microwave Power Amplifiers", *IEEE*

- Trans. On MTT*, vol. 47, No 12,  
pp.2364-2374, Dec. 1999
- [2] N. Carvalho and J. Pedro “Two-tone IMD asymmetry in microwave power amplifiers” *IEEE Trans. On MTT*, vol. 47, No 12, pp.445-448, Dec. 1999
  - [3] N. Carvalho and J. Pedro, “A Comprehensive Explanation of `Distortion Sideband Asymmetries” *IEEE Transactions On MTT*, Vol. 50, No. 9, September 2002. pp 2090-2101.
  - [4] J. Pedro and N. Carvalho, *Intermodulation Distortion in Microwave and Wireless Circuits*, Artech House, 2003.
  - [5] J. Vuolevi & T. Rahkonen. “*Distortions In RF Power Amplifiers*” Artech House, 2003.
  - [6] J.H.K. Vuolevi, T. Rahkonen, J.P.A. Manninen, “Measurement Technique for Characterizing memory Effects in RF Power Amplifier,” *IEEE Trans. MTT*, Vol. 49, No.8, pp. 1383-1389, Aug. 2001.

## Appendix A: Instrument set-up

### Front Panel set-up

#### ESG1 set-up (Master):

ESG1 will act as the master instrument. All triggering and the 10MHz reference oscillator frequency will be referenced to ESG1.

1. The first step is to initialize the instrument, usually by pressing 'Preset' or cycling the electrical power. Make sure that the RF is off after initialization.
2. Determine the input power range over which the DUT will be measured, taking into account any gain due to bench amplifier or cable loss. Set the amplitude range to approximately mid-range and turn attenuator hold 'ON' under the amplitude 'Ampl' menu.

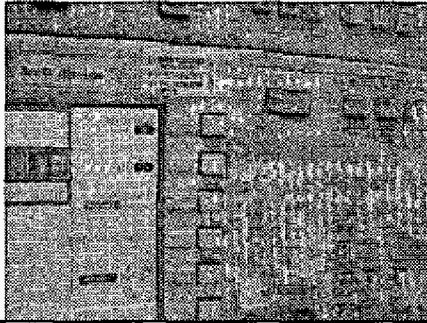


Figure A1  
Attenuator hold configuration

3. Switch the RF power 'ON' then, with the thumb wheel knob, scroll over the desired amplitude range making sure that an error is not displayed that indicates amplitude over or under range. If such an error does occur, expand or shrink the desired amplitude range. It should be noted that the desired amplitude range would be limited to the dynamic range of the ESG1 with attenuator hold 'ON'.
4. Configuring the instrument:
  - a) Go to the 'Sweep/List' menu
  - b) Set the 'Sweep' to amplitude sweep 'Ampl'
  - c) Set 'Sweep Type' to 'Step'
  - d) Set 'Sweep Repeat' to continuous 'Cont'
  - e) Then press 'Configure Step Sweep'

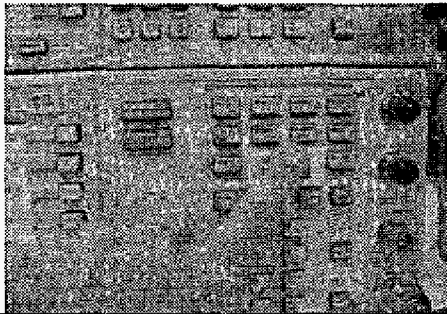


Figure A2  
Power sweep set-up

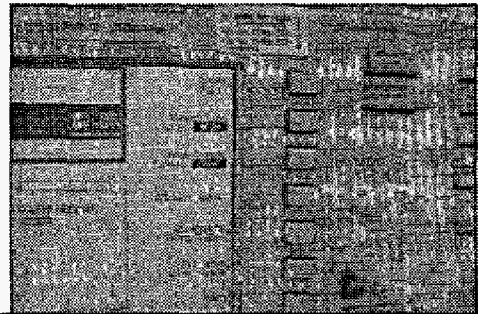
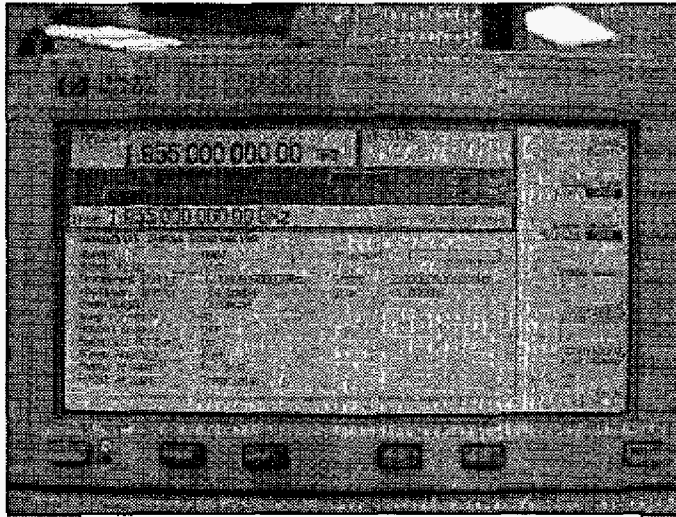


Figure A3  
Step sweep configuration

- e1) Select number of step points. For a 20dB range, 81 steps give 0.25dB resolution, i.e.  $20 \div 80 = 0.25\text{dB}$ . The extra point allows the instrument to start from the first chosen point.
- e2) Set dwell time.

If the dwell time step is set too small, a mismatch in the sweep time between the two signal generators is observed. Although in theory, the two instruments should be identical, in practice there are small



differences

Figure A4  
Dwell time set-up

especially if the models are different. A good dwell time was found to be in the region of 12mS. This value results in total sweep time of 972mS. This value is independent of carrier frequency separation.

- f) Press 'More (1 of 2)'
- g) Set 'Sweep Trigger' to 'Trigger' key
- h) leave 'Manual Mode' to 'Off' and 'Trigger Out Polarity' to 'Pos'
- i) Set the power 'Sweep Direction' to 'Up' or 'Down' as desired. One may want to examine the behavior of the DUT cooling down rather than heating up.

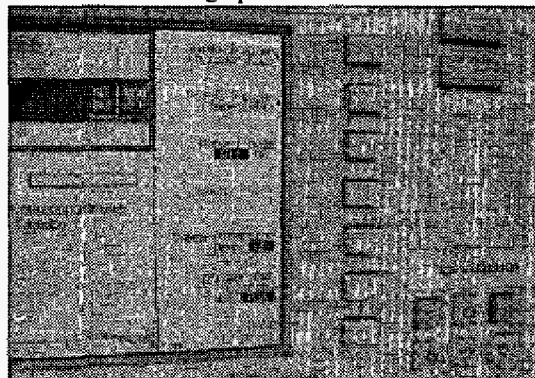


Figure A5  
Master sweep trigger set to 'key'

ESG 2 set-up (Slave):

Repeat all the setup steps as in ESG1 set-up with the exception of step 2-h. Here set the 'Sweep Trigger' to 'Ext Pos' or positive external triggering.

5. Set modulation to 'Mod Off' for both instruments.

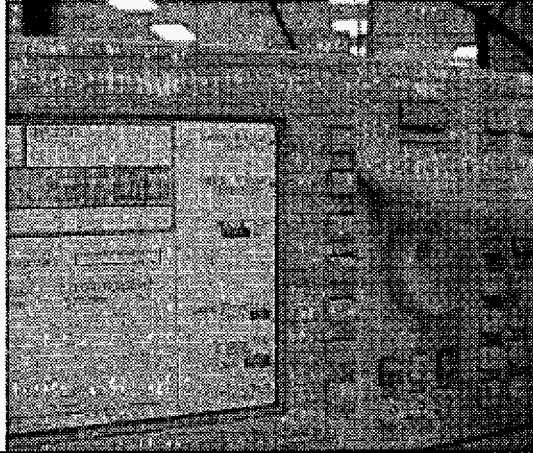


Figure A6  
Slave sweep trigger set to 'external'

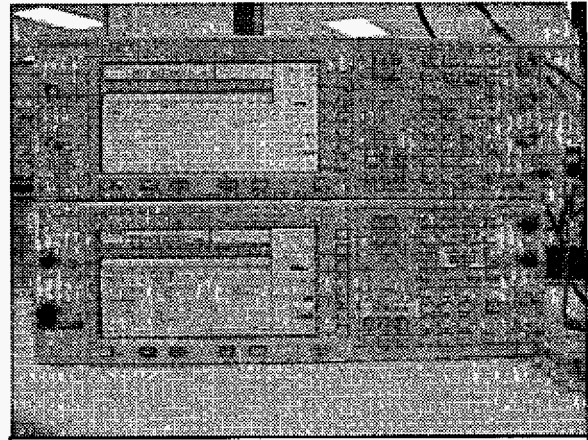


Figure A7  
Master-Slave signal generator stack

It should be noted that the RF carrier power level of each ESG at the input reference plane of the DUT is the same. This may require that the power range of each ESG should be set differently.

Vector Signal Analyzer (VSA):

The analyzer setup is as follows:

1. Initialize the instrument, usually by pressing 'Preset' or cycling the electrical power.
2. Set the instrument to 'Vector' mode.
3. Set the instrument 'Main Time'.
4. Select the Frequency-Under-Test (FUT), e.g. the frequency of the inter-modulation distortion product to be measured.
5. Set 'Span' to 750Hz.
6. Set 'num freq pts' to 1601.
7. Set 'main length' to 1.8s. This value is almost double that of the sweep time set for the ESG. There is a discrepancy between the cumulative dwell times of the ESG and the actual sweep time of the instrument. These values were found to be useful in the correct operation of the system. A little fine-tuning with the sweep time will be needed to get a precise end point. If the sweep time is not exact, the waveform will either run over the VSA display or not utilize the entire display. The case of a long VSA sweep time is shown below. These values are frequency independent.

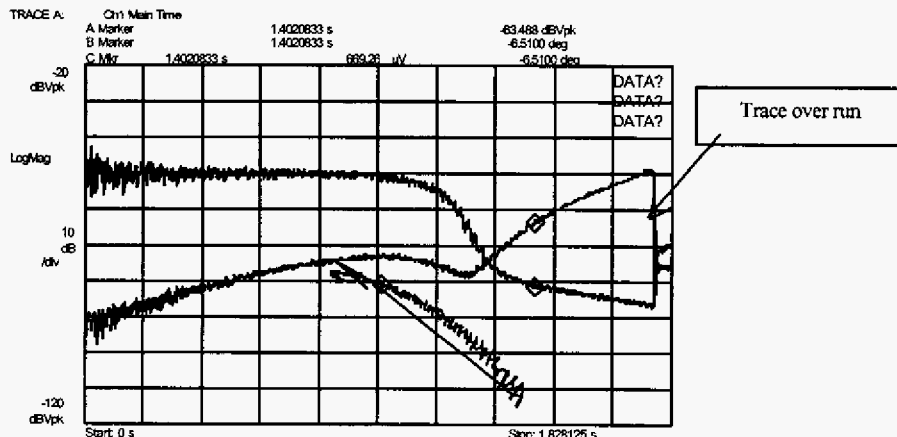


Figure A8  
The result of inaccurate sweep time set-up

8. These settings should give an 'RBW' of around 2Hz.
9. Set the 'Range' (i.e. amplitude) and 'Scale' appropriately so that the entire swept waveform is visible.
10. Set 'Trigger' to 'External'.

**Wiring connections**

The connection details and wiring picture are shown below:

Instrument name	Connection name	input/output	to/from
ESG1 (Master)	10MHz out	Output	ESG2
ESG1 (Master)	Trigger out	Output	ESG2/VSA
ESG2 (Slave)	10MHz in	Input	ESG1
ESG2 (Slave)	10MHz out	Output	VSA
ESG2 (Slave)	Trigger in	Input	ESG1
VSA1 (Slave)	10MHz in	Input	ESG2
VSA1 (Slave)	Trigger in	Input	ESG1

Table A1  
Master-Slave signal generator stack

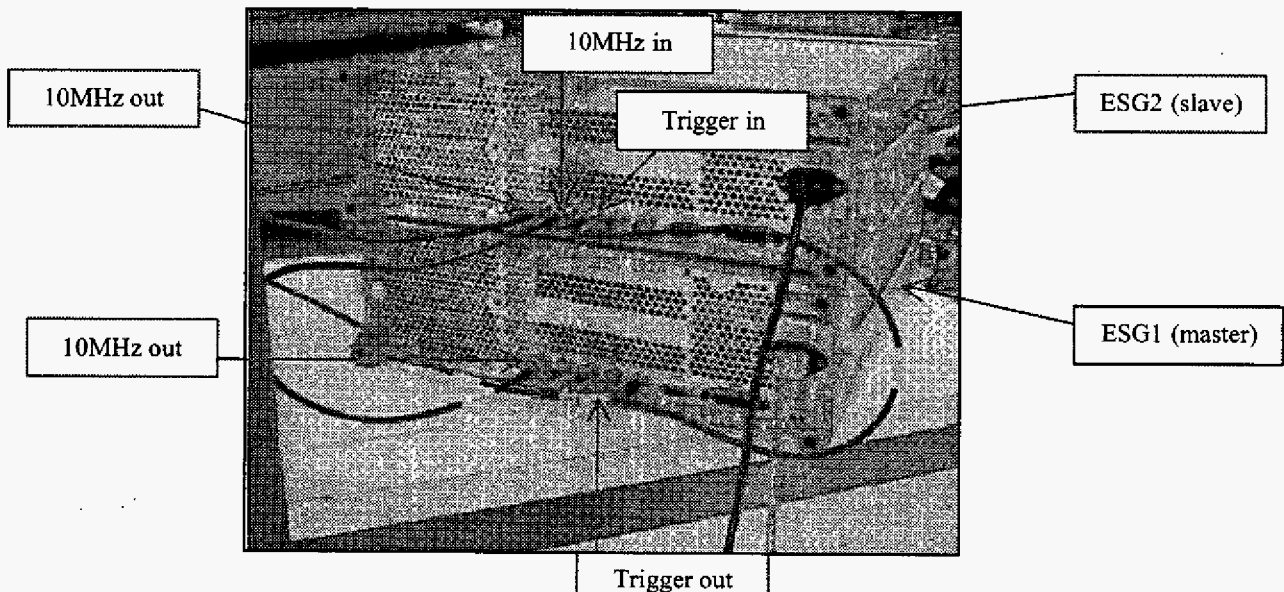


Figure A9  
ESG rear panel wiring diagram

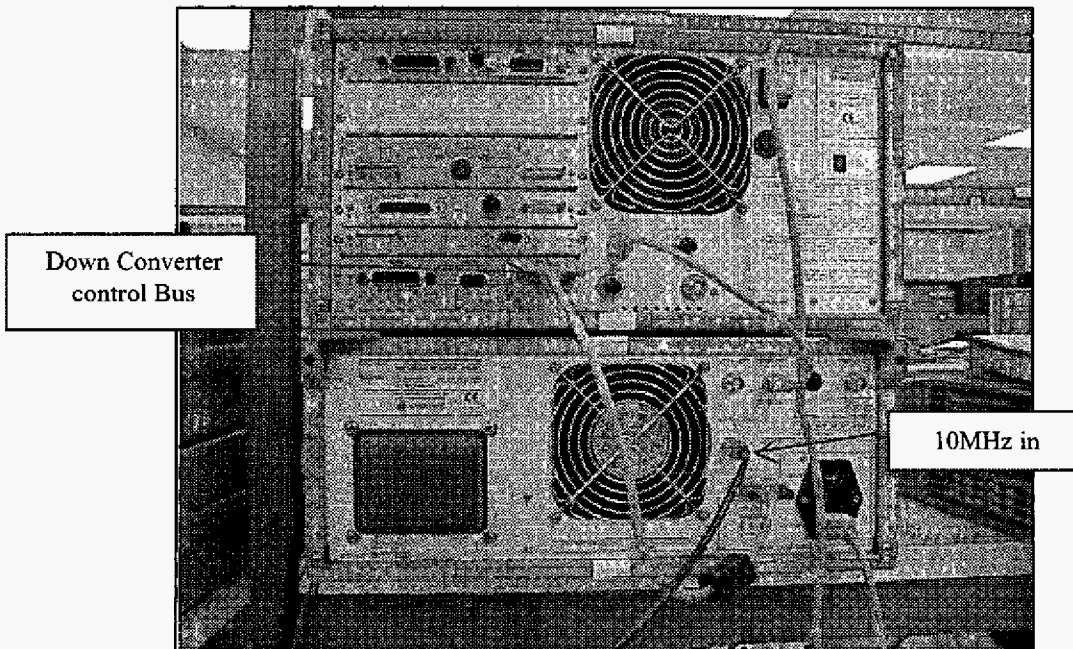


Figure A10  
VSA rear panel wiring diagram

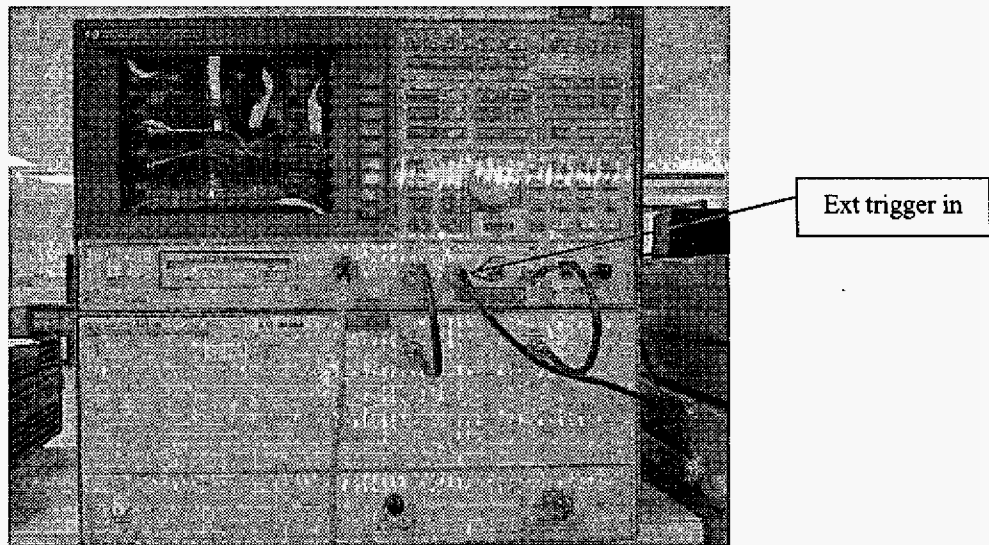


Figure A11  
VSA front panel wiring diagram

### **Operating the system**

Turn on the DUT and follow the instructions below:

1. Turn the RF power 'ON' on both ESG's.
2. Press the 'Trigger' key on the master ESG.

3. Observe the resultant waveform on the VSA.
4. Adjust parameter under test, e.g. bias current or drain voltage and repeat step 2&3.
5. Repeat as desired.

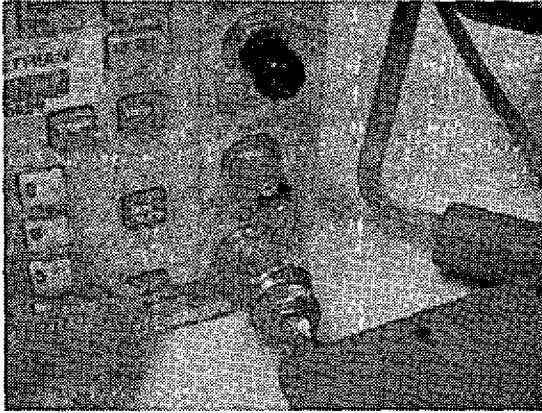


Figure A13  
Step 1: Switching RF power 'ON'

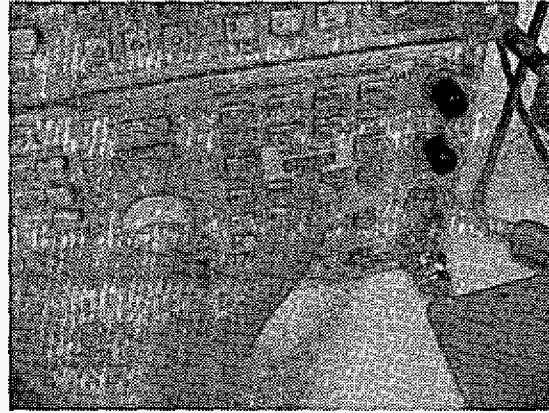


Figure A14  
Step 2: Triggering the source